

The Enhanced Electrochemical Properties of $\text{LiNi}_{0.6}\text{Co}_{0.2}\text{Mn}_{0.2}\text{O}_2$ Modified with Yttrium Oxide Coating as a Cathode Material for Lithium-Ion Batteries

Yuting Yang, Mingliang Yuan*, Guanjie Yan, Yaping Li, Yue Liu, Hanhui Liu, Tanxin Wang, ShuaiXie

School of Mineral Processing and Bioengineering, Central South University, Changsha, Hunan 410083, China

*E-mail: mlydoc@163.com

Received: 3 January 2020/ Accepted: 20 February 2020 / Published: 10 April 2020

Due to its high capacity and energy density, $\text{LiNi}_{0.6}\text{Co}_{0.2}\text{Mn}_{0.2}\text{O}_2$ is broadly regarded as one of the most promising active cathode materials in lithium-ion batteries. However, poor rate capability and cycling performance have significantly hindered the further commercialisation of $\text{LiNi}_{0.6}\text{Co}_{0.2}\text{Mn}_{0.2}\text{O}_2$. In this study, $\text{LiNi}_{0.6}\text{Co}_{0.2}\text{Mn}_{0.2}\text{O}_2$ is successfully modified by Y_2O_3 -coating in order to avoid negative side reactions between the electrodes and electrolytes, as well as to stabilise the cathode material's structure. The newly coated materials are characterised and investigated by several tests at high cut-off voltages. The hybrids with Y_2O_3 exhibit an excellent rate capability and outstanding cycling performance. Especially, they display a discharge capacity of 170.6 mAh g^{-1} with a retention of 85% after 100 cycles at 0.5 C over 3.0-4.6 V at room temperature. Therefore, the improved cathode material demonstrates excellent potential for application in the emerging green energy industry.

Keywords: Lithium-ion batteries; Y_2O_3 coating; High Voltage; Cathode materials

1. INTRODUCTION

Lithium-ion batteries (LIBs) have been extensively used in a wide range of electronic devices and hybrid electric vehicles[1, 2]. Recently, with global warming and the rising demand for green energy, the lithium-ion battery has been increasingly considered a promising alternative environmental-friendly energy source [3, 4]. Furthermore, of all the parts in LIBs, the electrodes play a very significant role in the core processes of lithium-ion intercalation and deintercalation[5, 6]. The research on anodes is developing rapidly, and many achievements have been made [7-9]. Regrettably, unlike anodes, the development of cathode materials has lagged. With lower toxicity, a low cost and a high reversible capacity, $\text{LiNi}_{1-x-y}\text{Co}_x\text{Mn}_y\text{O}_2$ (NCM) cathode materials have become a topical area in LIB research in recent years[10, 11]. In particular, with even higher theoretical capacity, Ni-rich $\text{LiNi}_{1-x-y}\text{Co}_x\text{Mn}_y\text{O}_2$ cathode materials are considered a viable alternative to LiCoO_2 , which has already been

used for conventional commercial products in LIBs since the 1990s [12, 13]. However, due to its insufficient capacity retention and poor rate capability, Ni-rich NCM materials still have many limitations in application[14]. Unsurprisingly, the stability of cathode materials decreases greatly over several uses[15].

To tackle these problems, various solutions, such as ion doping, concentration gradient structure and surface modification, have been utilised to improve the electrochemical performance of Ni-rich NCM cathode materials[16-19]. As one of the most efficient approaches, common surface coating including metal oxides (ZrO_2 , ZnO , Co_3O_4 , CeO_2 , TiO_2 , Al_2O_3 , RuO_2 and MoO_3)[20, 21], metal phosphates ($AlPO_4$, $LaPO_4$, $Mn_3(PO_4)_2$, and $Ni_3(PO_4)_2$)[22] and metal fluorides (MgF_2 , CeF_3 , AlF_3 , and FeF_3)[23], etc. could effectively improve the rate performance, reversible specific capacity, thermal stability and cycle performance of cathode materials[24]. In addition, surface modification can reduce the contact between cathode materials and air during mass production as well as extend storage life[25]. Among these modifier materials, metal oxides are widely used in the surface coating modification of NCM active materials[26]. As a traditional form of rare element oxides, yttrium oxide (Y_2O_3) shows excellent thermal stability, high corrosion resistance and good electrical contact with electrode materials. Therefore, Y_2O_3 may be a promising coating material for enhancing the electrochemical performance of LIBs. In the past few years, many articles on cathode materials have used Y_2O_3 as a modified additive, including $LiMn_2O_4$, $LiNi_{0.8}Co_{0.15}Al_{0.05}$, $LiNi_{0.5}Mn_{1.5}O_4$, $Li_{1.2}Mn_{0.54}Ni_{0.13}Co_{0.13}O_2$, $LiNi_{0.5}Co_{0.2}Mn_{0.3}O_2$ and $LiNi_{0.8}Co_{0.1}Mn_{0.1}O_2$, which prove that Y_2O_3 can truly help the battery retain a high capacity [27-30]. However, as a potential commercial material, the effect of nano-coated- Y_2O_3 on $LiNi_{0.6}Co_{0.2}Mn_{0.2}O_2$ cathodes during electrochemical performance has neither been researched nor reported on. And of all the relevant studies on Ni-rich cathode materials, the cycle performance and high rate capability of nano- Y_2O_3 -coating modified materials have yet to be investigated. The sol-gel process is a commonly used material preparation method, which is economical, allows for easy control of the morphology of synthetic materials and is very suitable for commercial manufacture. In this study, we used Y_2O_3 as a nano-coating to modify the surface environment of NCM622 particles through the wet method. The morphological and structural effects of yttrium oxide on a spherical NCM622 cover were investigated. Herein, the electrochemical and high cut-off voltage cycling properties of different amounts of Y_2O_3 coating on NCM622 were compared with the original bare active material.

2. EXPERIMENTAL SECTION

2.1. Material preparation

2.1.1. Preparation of $LiNi_{0.6}Co_{0.2}Mn_{0.2}O_2$

$LiNi_{0.6}Co_{0.2}Mn_{0.2}O_2$ precursor was synthesised by means of a co-precipitation method. Stoichiometric amounts of sulphate hydrate (mol% of $NiSO_4 \cdot 6H_2O$: $CoSO_4 \cdot 7H_2O$: $MnSO_4 \cdot 5H_2O$ = 6:2:2) were dissolved and stirred in deionised water to obtain a homogeneous solution. Then, the mixed metal salts solution was instilled into a continuous stirred tank reactor with appropriate amounts

of NaOH (as the precipitation) and NH_4OH (as the complexing agent) solution. The pH was carefully maintained at 11, and the temperature remained unchanged at 60°C during the whole process[31]. After six hours of vigorous stirring and reaction, the $\text{Ni}_{0.6}\text{Co}_{0.2}\text{Mn}_{0.2}\text{O}_2(\text{OH})_2$ precursor was obtained through extraction filtration, water washing and drying in a vacuum oven at 85°C for a suitable amount of time. Next, the dried precursor and $\text{LiOH}\cdot\text{H}_2\text{O}$ powder were mixed homogeneously at a molar ratio of 1:1.05. Subsequently, the mixture was preheated to 450°C for 5 h and calcined at 800°C for another 12 h. Ultimately, the NCM622 cathode material was prepared after naturally cooling it to room temperature.

2.1.2. Y_2O_3 coating on $\text{LiNi}_{0.6}\text{Co}_{0.2}\text{Mn}_{0.2}\text{O}_2$

The process of synthesising a Y_2O_3 -coated NCM622 sample is shown in Fig. 1. The concrete process is described as follows.

Firstly, 5 g of NCM622 powder and stoichiometric amounts of $\text{Y}(\text{NO}_3)_3\cdot 6\text{H}_2\text{O}$ were added into 300 and 200 ml of deionised water, and both were ultrasonically dispersed for 15 min, respectively. Then, with $\text{NH}_3\cdot\text{H}_2\text{O}$ as a chelating agent, the reaction environment pH was carefully controlled at 10.5 at 60°C , and the $\text{Y}(\text{NO}_3)_3$ solution was instilled into the $\text{LiNi}_{0.6}\text{Co}_{0.2}\text{Mn}_{0.2}\text{O}_2$ suspension at a speed of 1.5 mL/min. After continuously stirring for another 4 h, the insoluble resultant was water-washed several times and filtered and dried at 80°C in a vacuum oven for 12 h. In the end, the composite was sintered at 495°C for 6 h and cooled to room temperature. In this way, we successfully applied a Y_2O_3 coating to the NCM622 materials.

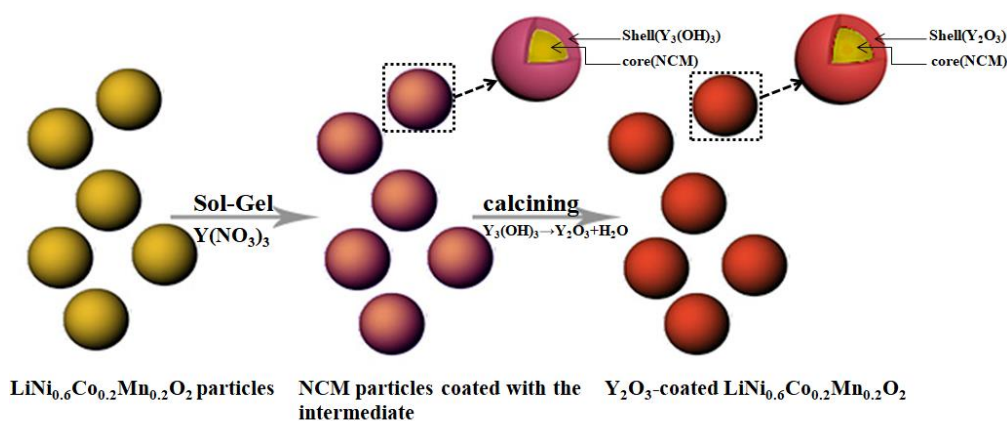


Figure 1. Schematic synthesis procedure of Y_2O_3 -coated NCM622.

2.2. Material characterisation

The crystalline phase, structure and compositions of the cathode materials were characterised by X-ray powder diffraction in the 2θ range of $5\text{--}80^\circ$ at a step size of 0.02° (XRD, DX-2700, Cu $\text{K}\alpha$ radiation). The morphological features of the samples were investigated by using scanning electron microscopy (SEM, TESCAN MIRA3 LMU) and high-resolution transmission electron microscopy

(HRTEM, Tecnai G2 F20). Energy dispersive spectroscopy (EDS, Oxford X-Max20) was tested in conjunction with SEM to ascertain the element content and distribution of the samples. X-ray photoelectron spectroscopy measurement was used to identify the chemical element state of the modified samples (XPS, ThermoFisher-VG Scientific ESCALAB250Xi, Inc) using monochromatic Al K α radiation ($h\lambda = 1486.6$ eV).

2.3. Electrochemical measurement

CR2025 coin cells were utilised in galvanostatic cycling to test the electrochemical performance of the samples. If not specially mentioned, all the processes of this part were finished at room temperature (25°C). 80 wt.% active material powder, 10 wt.% polyvinylidene fluoride (PVDF, as the binder) and 10 wt.% acetylene black (as the electrode precursor) were dissolved in N-methyl-2-pyrrolidone (NMP). The mixture slurry was pasted uniformly onto aluminium foil after grinding and was mixed well. Subsequently, the above cathode pieces were dried at 80 °C in the vacuum oven for 12 h and cut into wafers with a 14-mm diameter. With a treated cathode piece, a cut of lithium metal foil as the anode, a few drops of electrolyte (1 mol/L LiPF₆ in EC: EMC: DEC = 1:1:1 in volume) and Celgard 2400 as the separator, the cells were assembled in a glove box filled with high-purity argon. All the batteries were shelved for at least 12 h in air before the experiments. The cycling and rate performances of the cells were tested with the Neware Battery Test System BTS-XWJ-7.4.16S (Neware, China) at a range of 3.0-4.6 V. Cyclic voltammetry (CV) was performed at 0.1 mV s⁻¹ at a range of 2.8-4.6 V. Electrochemical impedance spectroscopy (EIS) measurements were carried out in a frequency range of 100 kHz to 10 mHz with an alternating current (AC) on an electrochemical workstation (GAMRY Reference 600).

3. RESULTS AND DISCUSSION

3.1. Material characterisation

As displayed in Fig. 2, the XRD patterns of samples (pristine NCM material and NCM material modified by Y₂O₃) showed similar sharp characteristic diffraction peaks corresponding to the hexagonal α -NaFeO₂ structure of the R3m space groups. The clear peak splitting of (006)/(002) and (108)/(110) demonstrates that both of the samples had a distinct layer structure. Moreover, a second phase appears. A new peak was detected at about 29°, which might be attributed to the characteristic peak of Y₂O₃, as the plane of (222) formed after the sample was calcined. Detailed data on the lattice parameters of the samples are given in Table 1.

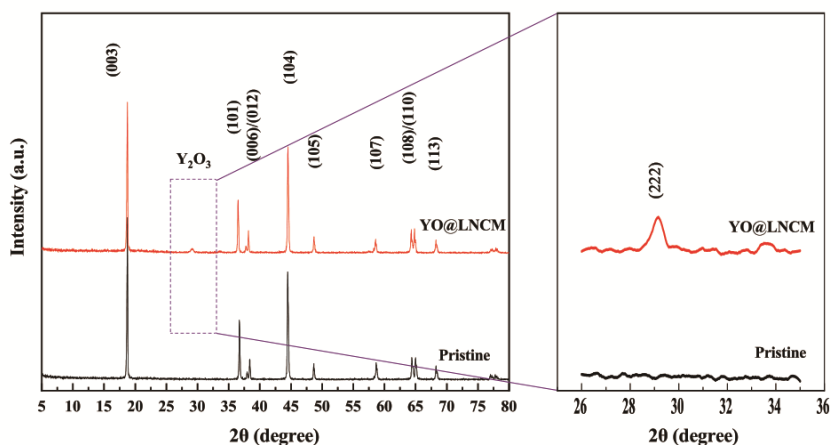


Figure 2. XRD patterns of pristine NCM and Y₂O₃-coated samples.

Table 1. Rietveld Refinement Results of XRD Data for Pristine NCM and Y₂O₃-Coated NCM.

	Pristine NCM	YO@LNCM
a(Å)	2.87974	2.8839
c(Å)	14.2273	14.3289
c/a	4.940	4.967
Unit	102.18	103.21
volume(Å ³)		
I(003)/(004)	1.5000	1.4079

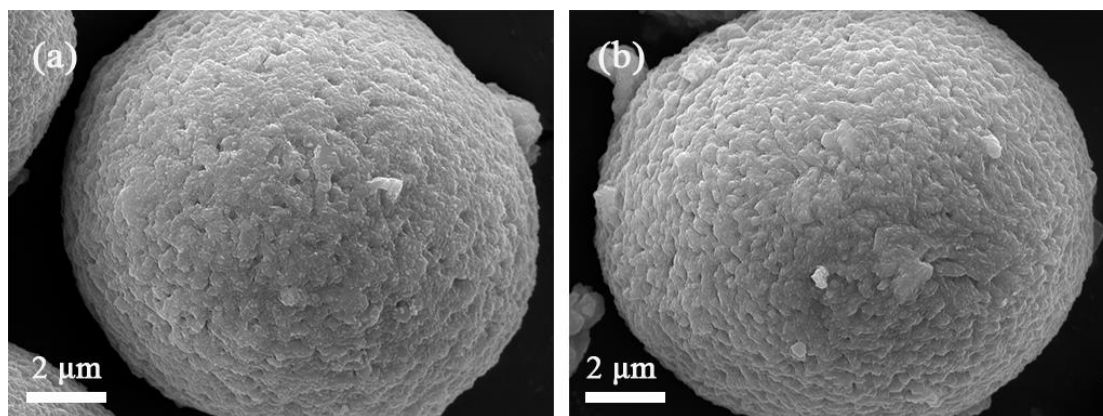


Figure 3. SEM images of (a) pristine NCM and (b) YO@LNCM.

The basic morphology of the samples was characterised by scanning electron microscopy (SEM) and is shown in Fig. 3. As can be seen in Fig. 3a, the bare NCM sample exists as a uniform-size spherical particle that has a comparatively smooth surface. Compared to Fig. 3b, which is an image of the modified sample, the particle surface is slightly rougher than that of the pristine active material, indicating that Y₂O₃ was coated onto the NCM particle surface successfully. The EDS mapping images were taken out to further express the distribution of metal elements on the surface, which are shown in

Fig. 4. From the mapping images of Ni, Co, Mn and Y in Fig. 4, we can see that the main modified cathode material elements, especially the element Y, are uniformly distributed, which reveals that Y_2O_3 was homogeneously coated onto the NCM particles.

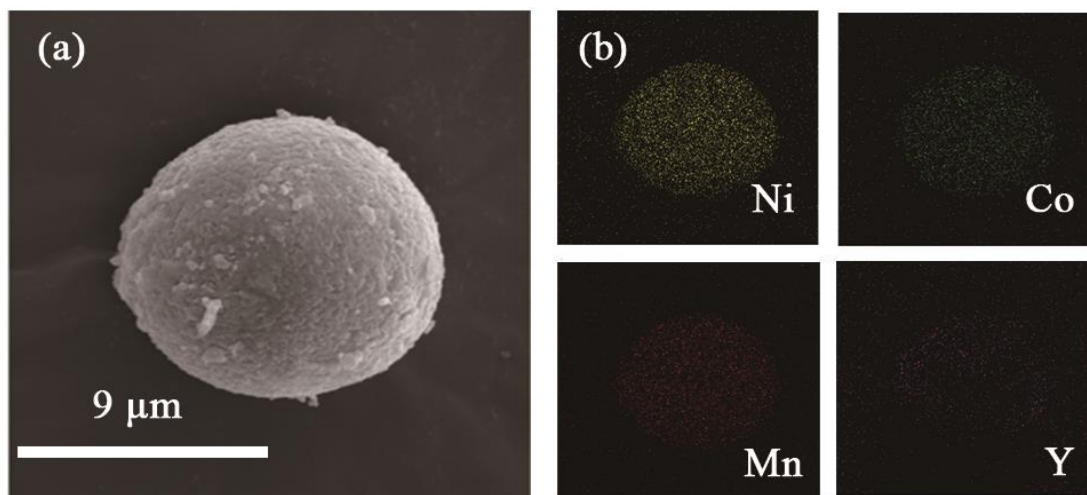


Figure 4. EDS elemental mapping results of YO@LNCM cathode materials.

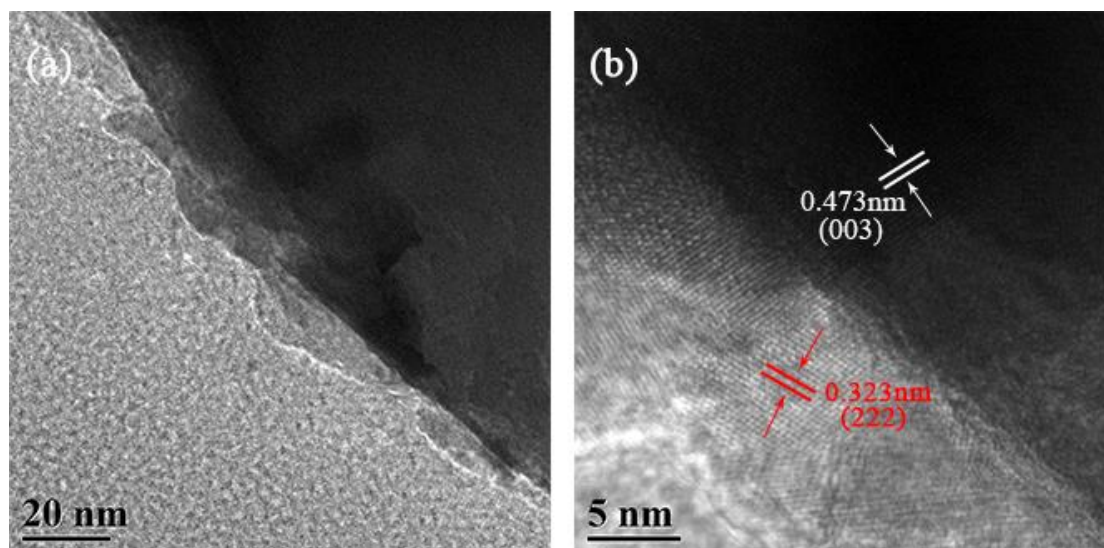


Figure 5. TEM images of YO@LNCM cathode material samples.

In order to observe the formation of modified samples more deeply, Fig. 5 shows HRTEM images of Y_2O_3 -coated NCM cathode materials at different magnifications. In the panels of Fig. 5a and 5b, Y_2O_3 was coated evenly onto the NCM particle surface in nanoscale, which is consistent with the SEM and EDS results. The lattice fringes of the edges on the sample in Fig. 5b with a white colour exhibit an inter-planar distance of 0.473 nm, which represents the (003) plane of NCM622. Meanwhile, the lattice fringes of the edges on the sample in Fig. 5b with a red colour exhibit an inter-planar distance of 0.323 nm, which is attributed to the (222) plane of the Y_2O_3 crystal. The appearance

of NCM's lattice fringes indicates that the surface coating modification did not change the existing crystal structure of the cathode material. Furthermore, the existence of Y_2O_3 lattice fringes coincides with SEM images, which confirms that Y_2O_3 was coated onto the active material.

To understand the newly synthesised oxides better, we used XPS to further investigate the valence state of YO@LNCM materials. Fig. 6 shows the XPS Y 3d spectra of the Y_2O_3 -coated NCM622 sample. In the chart, the Y 3d peaks show two peaks at 158.69 eV and 156.69 eV (the characteristic bonding energy of Y $3d_{5/2}$ and Y $3d_{3/2}$, respectively), which means that the coating process did not alter the oxidation state of the element Y.

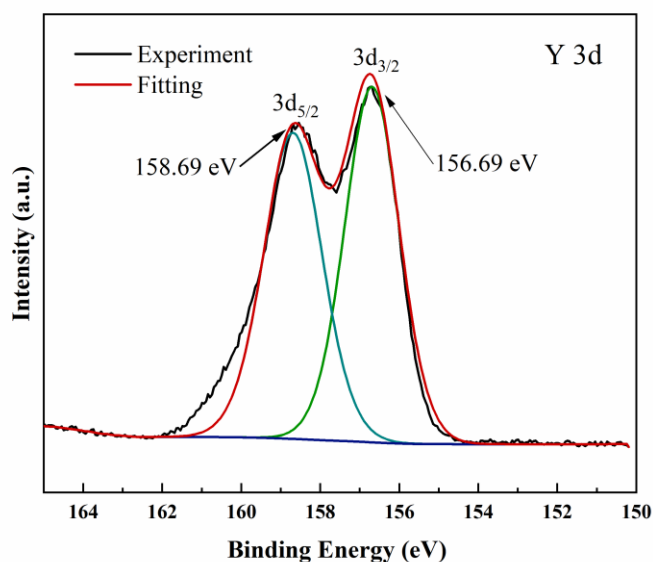


Figure 6. The XPS analysis of the modified NCM622 (Y 3d spectra).

3.2. Electrochemical performance

Fig. 7 shows the initial charge-discharge curves of the pristine and the modified sample at a current density of 0.1 C within a voltage range of 3.0-4.6 V. We can see from the image that the pristine and YO@LNCM (Y_2O_3 -coated NCM622 sample) fall under similar curves in the initial charge/discharge processes. The lack of obvious differences indicates that yttrium oxide coating did not obstruct lithium-ion normal exertion/insertion in the cathode material. In addition, with the appearance of yttrium oxide, the initial discharge capacity decreased. This is likely because Y_2O_3 is a form of inactive oxide, and it is not effective at conducting electrons during the charged-discharged process[32, 33]. Besides, the initial charge/discharge capacities of the pristine NCM622 and YO@LNCM were 228.4/222.1 mAh g^{-1} and 227.0/213.3 mAh g^{-1} , while their initial coulombic efficiencies were 97.2 % and 94.0 %, respectively.

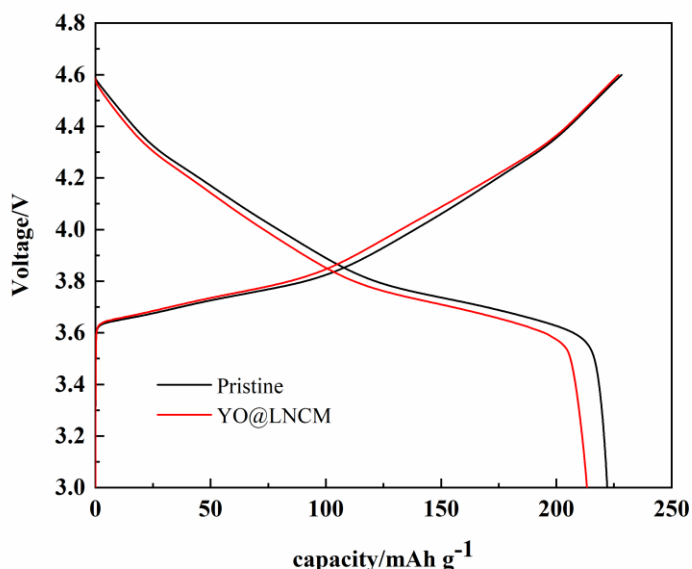


Figure 7. Initial charge/discharge curve of pristine and Y_2O_3 -coated samples.

To evaluate the cycle performances of the pristine and Y_2O_3 -coated NCM622 samples, the pristine and YO@LNCM samples were charged-discharged at 0.5 C between 3.0 and 4.6 V for 100 cycles (Fig. 8). After that, the discharge capacity of the pristine sample was 136.7 mAh g^{-1} , and it had a capacity retention rate of 66.5%. Compared to the bare sample, the YO@LNCM product showed a higher discharge capacity and capacity retention, which was 170.6 mAh g^{-1} at a rate of 85.4%. The higher capacity retention of the modified sample indicates that the appearance of a protective layer suppressed the side reactions. A physical barrier was built at the interface between the cathode material and the electrolyte to avoid direct contact between the two[34]. These improvements enhanced the cell cycling process.

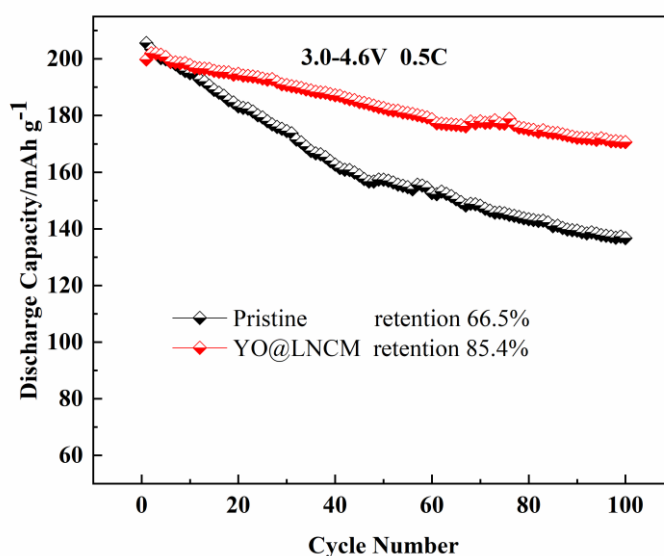


Figure 8. Electrochemical performance (100 cycles at 0.5 C) of NCM622 (black symbol) and Y_2O_3 -coated NCM622 samples (red symbol).

The rate capabilities of the pristine and modified samples are compared in Fig. 9. All the half cells were tested under discharge rates of 0.2, 0.5, 1, 2, 5 and 0.2 C at 3.0-4.6 V at room temperature, respectively. And as Fig. 9 shows, at 0.2 C, the discharge capacity of the pristine was slightly higher than that of the modified samples. This is also because yttrium oxide showed no electrochemical activity within the given voltage range[35]. However, at other discharge rates, the YO@LNCM sample performed better than the bare NCM material did. Particularly, while the pristine sample performed very poorly at a high rate discharge of 5 C, the modified sample exhibited a 30-mAh g⁻¹ higher discharge capacity than the original discharge capacity of 123.4 mAh g⁻¹. The coated samples' varying multiplier performance demonstrates that proper Y₂O₃ coating can improve the LIB's capability by protecting the electrodes from side reactions, lowering the surface residual lithium salts and improving the reversible transfer of Li⁺[36]. The rate capabilities result herein is consistent with that of previous performance studies.

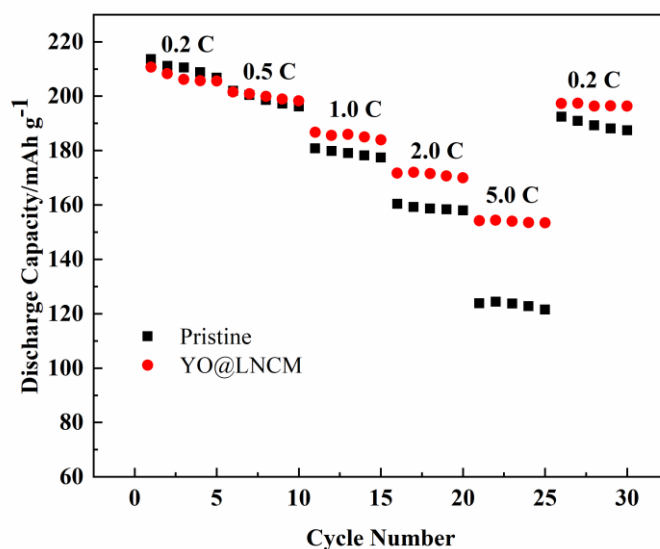


Figure 9. Rate capabilities of the pristine and Y₂O₃-coated NCM samples.

A comparison of the electrochemical performance of similar yttrium oxide-coated cathode materials used for lithium-ion batteries is shown in Table 3. As can be clearly observed, after 50 cycles, the capacity retention rate of YO@LNCM622 was much higher than that of YO@LNCM523 and YO@LNCA. And after 100 cycles, the capacity retention rate of YO@LNCM (high cut-off voltage) was slightly lower than that of YO@LNCM811 and Li_{1.2}Mn_{0.54}Ni_{0.13}Co_{0.13}O₂ materials (normal cut-off voltage), which was caused by the difference in cut-off voltage. Increasing the charging voltage means that more Li⁺ is removed from the cathode electrode so that the transition metal element in the cathode electrode has a higher valence state. Therefore, a high cut-off voltage usually leads to a decrease in the structural stability of the material itself and a decrease in the stability of the material/electrolyte interface. As a result, considering various situations, we believe that the cycling performance of YO@LNCM cathode material is excellent.

Table 3. The electrochemical properties of typical Y_2O_3 -coated NCM/NCA cathode materials.

Samples	Initial discharge capacity/mAh g^{-1}	Coulombic efficiency	Capacity Retention rate	Reference
YO@LNCM622	213.3 (0.5 C)	94.0 %	93.9 % after 50 cycles 85.4 % after 100 cycles	This work
YO@LNCM811	188.9 (0.1 C)	85.5 %	91.4% after 100 cycles	[29]
YO@ $\text{Li}_{1.2}\text{Mn}_{0.54}\text{Ni}_{0.13}\text{Co}_{0.13}\text{O}_2$	280.3 (0.1 C)	82.3 %	89.1 % after 200 cycles	[27]
YO@LNCM523	182.5 (1 C)	No report	87.8 % after 50 cycles	[28]
YO@LNCA	195.0 (0.5C)	No report	93.0 % after 50 cycles	[30]

Fig. 10(a, b) displays the first, second and third cyclic voltammograms of the pristine and Y_2O_3 -coated NCM622 samples, respectively, which were recorded within a voltage range of 2.8-4.6 V at a scan rate of 0.1 mV s^{-1} . The diagram shows that the redox peaks of the samples were similar in shape, indicating that the Y_2O_3 modification had little effect on the electrochemical reaction core process. At the same time, according to the decrease in irreversible impedance, the oxidation peaks and reductions peaks were tuned to a low voltage with gradually increasing charge-discharge cycles. The potential difference value ΔE shows the difference between the oxidation peak and reduction peak in the same cycle. In addition, the value of ΔE represents the degree of electrochemical reversibility[37]. Also, it is important to note that the YO@LNCM cathode materials had sharper oxidation peaks, indicating better conductivity on coating materials [38]. As shown in Fig. 10, the first to the third cycles of ΔE values in the Y_2O_3 -coated sample were much lower than that of the pristine sample ($0.415 \text{ V}/0.223 \text{ V}$, $0.155 \text{ V}/0.143 \text{ V}$, and $0.136 \text{ V}/0.135 \text{ V}$), which means that the distance from the oxidation peak to the reduction peak in the same cycle was shortened, implying that Y_2O_3 coating improves the reversibility of electrochemical reactions.

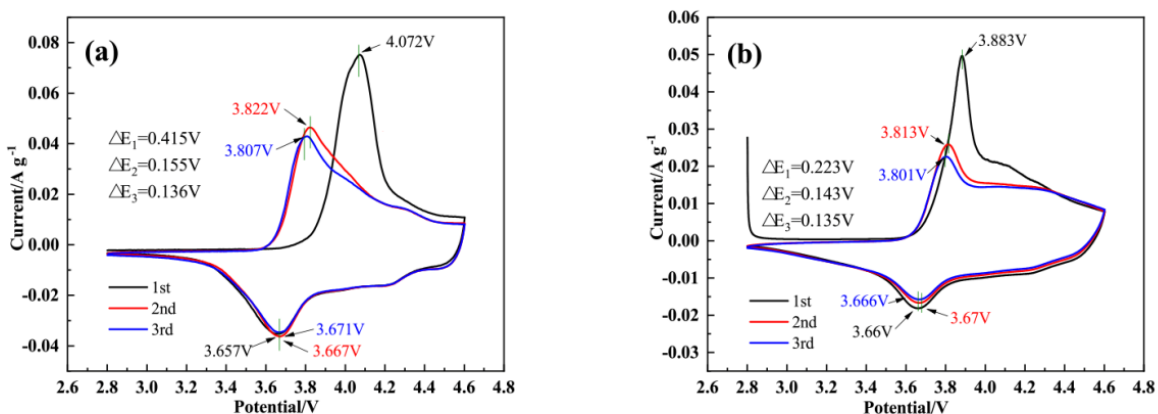
**Figure 10.** Cyclic voltammetry measurements for NCM622 (a) and Y_2O_3 -coated NCM622 samples (b) with a scan rate of 0.1 mV s^{-1} .

Fig. 11 shows the electrochemical impedance spectroscopies (EIS) of the modified NCM622 sample and the pristine one. All the batteries were charged to 4.6 V, at 0.1 C, respectively. Note that each Nyquist plot has one semicircle at a high-to-medium frequency and one oblique line at a low frequency. The fitting equivalent circuit models are also displayed in Fig. 11. In the diagram, the slight interruption came from the solution and battery components' internal resistance (R_s), which was similar for both samples. Meanwhile, the semicircle is represented by R_{ct} , which closely corresponded to the impedance of the charge transfer. The quasilinear part of the curve is primarily related to the diffusion of Li^+ , which is usually called the Warburg impedance (W_0)[39].

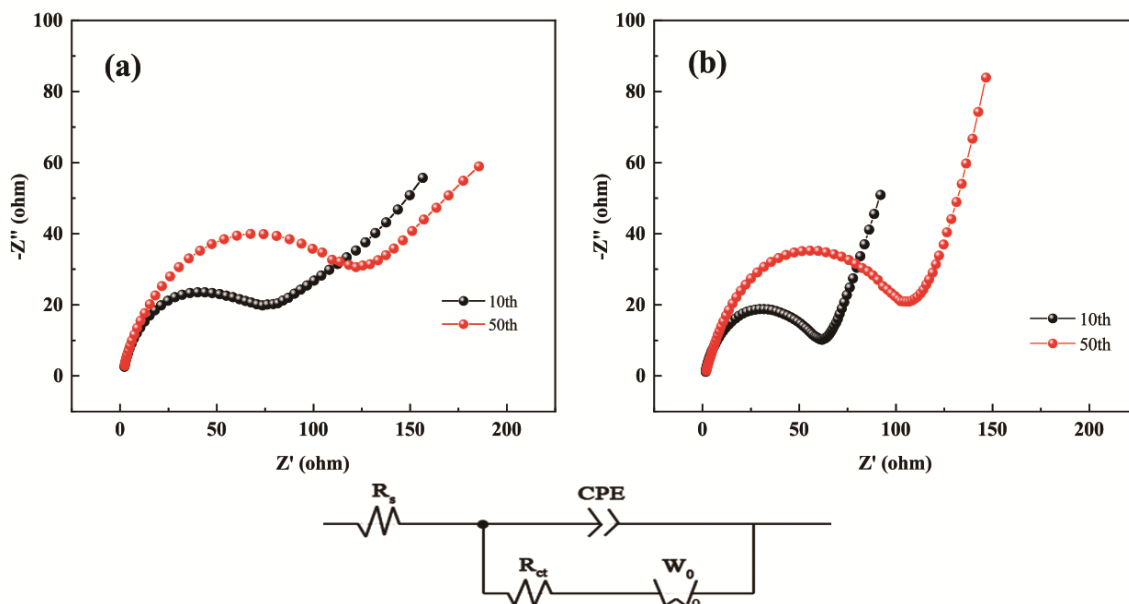


Figure 11. Electrochemical impedance spectroscopy of pristine and Y_2O_3 -coated NCM cathodes.

As a supplement, the fitted values of R_s and R_{ct} are shown in Table 2. The CPE shows the non-ideal capacitance of the surface layer[40]. As observed in Table 2, from the 10th cycle to the 50th cycle, the values of R_{ct} rose rapidly, and the pristine sample's values increased faster than that of YO@LNCM (from 64.18 Ω to 103.2 Ω , from 43.44 Ω to 66.28 Ω , respectively). Meanwhile, both samples' internal resistances (R_s) remained almost the same after the cycles. Less impedance means better stability of NCM and the NCM/electrolyte interface and better reversibility during electrochemistry reactions[41]. Therefore, the results further verify that the Y_2O_3 coating could suppress the interfacial side reactions and stabilise the cathode's structure to improve the conduction of lithium ions.

Table 2. Fitting results of R_s and R_{ct} of pristine and Y_2O_3 -modified $LiNi_{0.6}Co_{0.2}Mn_{0.2}O_2$ samples.

Samples	R_s (Ω)		R_{ct} (Ω)	
	10th	50th	10th	50th
$LiNi_{0.6}Co_{0.2}Mn_{0.2}O_2$	3.038	3.468	64.18	103.2
YO@LNCM	2.142	2.849	43.44	66.28

4. CONCLUSIONS

In summary, we successfully designed and synthesised Y_2O_3 -modified $\text{LiNi}_{0.6}\text{Co}_{0.2}\text{Mn}_{0.2}\text{O}_2$ cathode materials for the first time, demonstrating a significantly improved electrochemical performance at a high cut-off voltage. The application of a moderate Y_2O_3 coating layer onto a $\text{LiNi}_{0.6}\text{Co}_{0.2}\text{Mn}_{0.2}\text{O}_2$ cathode was demonstrated by XRD, SEM, EDS, HRTEM and XPS studies. The Y_2O_3 -coated NCM622 showed an excellent capacity retention of 85.4% (170.6 mAh g^{-1}) compared to an original capacity retention of 66.5% (136.7 mAh g^{-1}) after 100 cycles at 0.5 C and exhibited an outstanding rate performance compared to the pristine sample at a high current density. Our results indicate that Y_2O_3 coating could suppress the side reactions between electrodes and electrolytes and stabilise the structure of the positives effectively. Our results suggest that a proper amount of Y_2O_3 coating could constitute a promising NCM622 cathode material modifier with enhanced properties in Li-ion batteries.

ACKNOWLEDGMENTS

This work was supported by the Major Science and Technology Research of Guangxi Department of Funded Projects (Grant No.1114022-15).

CONFLICT OF INTEREST

We declare that we do not have any commercial or associative interest that represents a conflict of interest in connection with the work submitted.

References

1. W.Waag, C. Fleischer, D.U. Sauer, *J. Power Sources*, 258 (2014) 321-339.
2. M.A. Hannan, M.S.H. Lipu, A. Hussain, A. Mohamed, *Renewable and Sustainable Energy Rev.*, 78 (2017) 834-854.
3. D. Andre, S. Kim, P. Lamp, S.F. Lux, F. Maglia, O. Paschos, B. Stiaszny, *J. Mater. Chem. A*, 3 (2015) 6709-6732.
4. C.P. Grey, J.M. Tarascon, Sustainability and in situ monitoring in battery development, *Nat. Mater.*, 16 (2017) 45-56.
5. J. Shi, D. Xiao, M. Ge, X. Yu, Y. Chu, X. Huang, X. Zhang, Y. Yin, X. Yang, Y. Guo, L. Gu, L. Wan, *Adv. Mater.*, 30 (2018) 1705575.
6. J. Zheng, J.A. Lochala, A. Kwok, Z.D. Deng, J. Xiao, *Adv. Sci.*, 4 (2017) 1700032.
7. Y.-Q. Li, J.-C. Li, X.-Y. Lang, Z. Wen, W.-T. Zheng, Q. Jiang, *Adv. Funct. Mater.*, 27 (2017) 1700447.
8. X. Shen, Z. Tian, R. Fan, L. Shao, D. Zhang, G. Cao, L. Kou, Y. Bai, *J. Energy. Chem.*, 27 (2018) 1067-1090.
9. M. Li, J. Lu, Z. Chen, K. Amine, *Adv. Mater.*, 30 (2018) 1800561.
10. F.A. Susai, H. Sclar, Y. Shilina, T.R. Penki, R. Raman, S. Maddukuri, S. Maiti, I.C. Halalay, S. Luski, B. Markovsky, D. Aurbach, *Adv. Mater.*, 30 (2018) 1801348.
11. H. Zhang, H. Zhao, M.A. Khan, W. Zou, J. Xu, L. Zhang, J. Zhang, *J. Mater. Chem. A*, 6 (2018) 20564-20620.
12. T. Kim, W. Song, D.-Y. Son, L.K. Ono, Y. Qi, *J. Mater. Chem. A*, 7 (2019) 2942-2964.
13. J. Kim, H. Lee, H. Cha, M. Yoon, M. Park, J. Cho, *Adv. Energy Mater.*, 8 (2018) 1702028.

14. Y. Xia, J. Zheng, C. Wang, M. Gu, *Nano Energy*, 49 (2018) 434-452.
15. L. de Biasi, B. Schwarz, T. Brezesinski, P. Hartmann, J. Janek, H. Ehrenberg, *Adv. Mater.*, 31 (2019) 1900985.
16. Z. Chen, D. Chao, J. Lin, Z. Shen, *Mater. Res. Bull.*, 96 (2017) 491-502.
17. K. Hoang, *Phys. Rev. Mater.*, 1 (2017) 075403.
18. Y. Sun, Z. Zhang, H. Li, T. Yang, H. Zhang, X. Shi, D. Song, L. Zhang, *Dalton Trans*, 47 (2018) 16651-16659.
19. X. Xu, J. Jian, L. Xiang, L. Wang, X. He, G. Yin, C. Du, *Electrochim. Acta*, 317 (2019) 459-467.
20. M.K. Shobana, *J. Alloys Compd.*, 802 (2019) 477-487.
21. D. Zuo, C. Wang, G. Tian, K. Shu, X. Liu, *J. Electrochem. Sci. Eng.*, 9 (2019) 85.
22. Z. Chen, G. Kim, Y. Guang, D. Bresser, T. Diemant, Y. Huang, M. Copley, R. J. Behme, S. Passerini, Z. Shen, *J. Power Sources*, 402 (2018) 263-271.
23. A. Shapira, O. Tiurin, N. Solomatin, M. Auinat, A. Meitav, Y. Ein-Eli, *ACS Appl. Energy Mater.*, 1 (2018) 6809-6823.
24. F. Schipper, P. Nayak, E. Erickson, S. Amalraj, O. Srur-Lavi, T. Penki, M. Talianker, J. Grinblat, H. Sclar, O. Breuer, C. Julien, N. Munichandraiah, D. Kovacheva, M. Dixit, D. Major, B. Markovsky, D. Aurbach, *Inorganics*, 5 (2017) 32.
25. J.T. Zhang, X.H. Tan, L.M. Guo, Y. Jiang, S.N. Liu, H.F. Wang, X.H. Kang, W.G. Chu, *J. Alloys Compd.*, 771 (2019) 42-50.
26. L. Xu, F. Zhou, B. Liu, H. Zhou, Q. Zhang, J. Kong, Q. Wang, *Int. J. Electrochem.*, 2018 (2018) 1-12.
27. Q. Chen, L. Luo, L. Wang, T. Xie, S. Dai, Y. Yang, Y. Li, M. Yuan, *J. Alloys Compd.*, 735 (2018) 1778-1786.
28. J. Xu, X. Chen, C. Wang, L. Yang, X. Gao, Y. Zhou, K. Xiao, X. Xi, *Ceram. Int.*, 43 (2017) 11848-11854.
29. S. Dai, M. Yuan, L. Wang, L. Luo, Q. Chen, T. Xie, Y. Li, Y. Yang, *Ceram. Int.*, 45 (2019) 674-680.
30. M.M. Loghavi, H. Mohammadi-Manesh, R. Eqra, *J. Electroanal. Chem.*, 848 (2019) 113326.
31. H. Yang, K. Du, Z. Peng, Y. Cao, K. Wu, Y. Lu, X. Qi, K. M, J. Wu, *Electrochim. Acta*, 289 (2018) 149-157.
32. S. Dong, Y. Zhou, C. Hai, J. Zeng, Y. Sun, Y. Shen, X. Li, X. Ren, G. Qi, X. Zhang, L. Ma, *Ceram. Int.*, 45 (2019) 144-152.
33. X. Jiang, *Int. J. Electrochem. Sci.*, (2018) 2341-2354.
34. Y. Huang, J. Xia, G. Hu, Y. Cao, Z. Peng, J. Fan, Y. Tao, T. Li, Z. Zhang, Z. Xue, K. Du, *Electrochim. Acta*, 332 (2020) 135505.
35. Z. Gan, G. Hu, Z. Peng, Y. Cao, H. Tong, K. Du, *Appl. Surf. Sci.*, 481 (2019) 1228-1238.
36. Q. Jiang, H. Yu, Y. Hu, H. Jiang, C. Li, *Ind. Eng. Chem. Res.*, 58 (2019) 23099-23105.
37. L. Li, Z. Zhang, S. Fu, Z. Liu, Y. Liu, *J. Alloys Compd.*, 768 (2018) 582-590.
38. Y. Ding, B. Deng, H. Wang, X. Li, T. Chen, X. Yan, Q. Wan, M. Qu, G. Peng, *J. Alloys Compd.*, 774 (2019) 451-460.
39. L. Xu, F. Zhou, H. Zhou, J. Kong, Q. Wang, G. Yan, *Electrochim. Acta*, 289 (2018) 120-130.
40. M. Zhang, H. Zhao, M. Tan, J. Liu, Y. Hu, S. Liu, X. Shu, H. Li, Q. Ran, J. Cai, X. Liu, *J. Alloys Compd.*, 774 (2019) 82-92.
41. Y. Wu, H. Ming, M. Li, J. Zhang, W. Wahyudi, L. Xie, X. He, J. Wang, Y. Wu, J. Ming, *ACS Energy Lett.*, 4 (2019) 656-665